entropy

MDPI

Article

Fractal and Entropy Analysis of the Dow Jones Index Using Multidimensional Scaling

José A. Tenreiro Machado

Department of Electrical Engineering, Institute of Engineering, Polytechnic Institute of Porto, 4249-015 Porto, Portugal; jtm@isep.ipp.pt; Tel.: +351-228340500

Received: 4 September 2020; Accepted: 30 September 2020; Published: 8 October 2020

Abstract: Financial time series have a fractal nature that poses challenges for their dynamical characterization. The Dow Jones Industrial Average (DJIA) is one of the most influential financial indices, and due to its importance, it is adopted as a test bed for this study. The paper explores an alternative strategy to the standard time analysis, by joining the multidimensional scaling (MDS) computational tool and the concepts of distance, entropy, fractal dimension, and fractional calculus. First, several distances are considered to measure the similarities between objects under study and to yield proper input information to the MDS. Then, the MDS constructs a representation based on the similarity of the objects, where time can be viewed as a parametric variable. The resulting plots show a complex structure that is further analyzed with the Shannon entropy and fractal dimension. In a final step, a deeper and more detailed assessment is achieved by associating the concepts of fractional calculus and entropy. Indeed, the fractional-order entropy highlights the results obtained by the other tools, namely that the DJIA fractal nature is visible at different time scales with a fractional order memory that permeates the time series.

Keywords: multidimensional scaling; fractals; fractional calculus; financial indices; entropy; Dow Jones; complex systems

1. Introduction

The Dow Jones Industrial Average (DJIA), or Dow Jones, is a stock market index that reflects the stock performance of 30 relevant companies included in the U.S. stock exchanges. The DJIA is the second-oldest among the U.S. market indices and started on 26 May 1896. The DJIA is the best-known index in finance and is considered a key benchmark for assessing the global business trend in the world.

The financial time series reflect intricate effects between a variety of agents coming from economic and social processes, geophysical phenomena, health crisis, and political strategies [1–4]. At present, we find all sorts of financial indices for capturing the dynamics of markets and stock exchange institutions. In general, all have a fractal nature with variations that are difficult to predict [5–13]. A number of techniques have been proposed to investigate the financial indices and to unravel the embedded complex dynamics [14–18]. Such studies adopt the underlying concept of linear time flow and consider that the fractal nature of the index is intrinsic to its own artificial nature.

This paper studies the interplay between the DJIA values and the time flow. The present day standard assumption is that time is a continuous linear succession of events often called the "arrow of time". We must clarify that (i) the nature of the time variable, either continuous or discrete, either with a constant rhythm of variation or not, is simply under the light of the financial index, so that we are independent of the classical laws of physics, (ii) merely the DJIA is adopted since other financial indices reveal the same type of behavior, but are limited to much shorter time series, and (iii) no financial

foreseeing is intended. Therefore, the Gedankenexperiment in the follow-up addresses the controversy about the texture of time [19–22], but just in the limited scope of financial indices.

For this purpose, the concepts of multidimensional scaling (MDS), fractional dimension, entropy, and fractional calculus are brought up as useful tools to tackle complex systems. MDS is a computational tool for visualizing the level of similarity between items of a dataset. The MDS translates information regarding the pairwise distances among a set of items into a configuration of representative points of an abstract Cartesian space [23–29]. Mandelbrot coined the word "fractal" [30,31] for complex objects that are self-similar across different scales. Fractals can be characterized by the so-called fractal dimension, which may be seen as quantifying complexity [32–34]. Information theory was introduced by Claude Shannon [35] and has as the primary concept the information content of a given event, which is a decreasing function of its probability [36–39]. The entropy of a random variable is the average value of information and has been proven to be a valuable tool for assessing complex phenomena [40–42]. Fractional calculus (FC) is the branch of mathematical analysis that generalizes differentiation and integration to real or complex orders [43–48]. The topic was raised by Gottfried Leibniz in 1695 and remained an exotic field until the Twentieth Century. In the last few decades, FC became a popular tool for analyzing phenomena with long-range memory and non-locality [49–57].

The association of these mathematical and computational tools yields relevant viewpoints when analyzing financial indices [7–9,11,58–61].

Bearing these ideas in mind, this paper is organized as follows. Section 2 introduces the dataset and methods and develops some initial experiments using MDS. Section 3 explores the use of fractal and entropy analysis of the MDS loci. Finally, Section 4 draws the main conclusions.

2. Dataset and Methods

2.1. The DJIA Dataset

The dataset consists of the daily close values of the DJIA from 28 December 1959, up to 1 September 2020, corresponding to a time series of $T = 15{,}832$ days, covering approximately half a century. Each week consists of 5 working days, and some missing data due to special events were estimated by means of linear interpolation between adjacent values.

We assess the dynamics of the DJIA by comparing its values $x(t)$ for a given time window of t_w days. Therefore, the ith vector of DJIA values consists of $\xi_i = [x(1), \ldots, x(t_w)]$, where days "1" and "$t_w$" denote the start and end time instants in the time window. Hereafter, for simplicity, we consider consecutive disjoint time windows, and a number of experiments with t_w having values multiples of 5 days. Therefore, the total number of time windows (and vectors) is $N_w = \left\lfloor \frac{T}{t_w} \right\rfloor$, where $\lfloor \cdot \rfloor$ denotes the floor function, which gives as the output the greatest integer less than or equal to the input value.

The evolution of the DJIA in time reveals a fractal nature as represented in Figure 1. If we calculate the histogram of the logarithm of the returns, that is of $lr = \ln\left(\frac{x(t+1)}{x(t)}\right)$, we verify a sustained noisy behavior and fat tails in the statistical distribution as depicted in Figure 2 for time windows of $t_w = 60$ days.

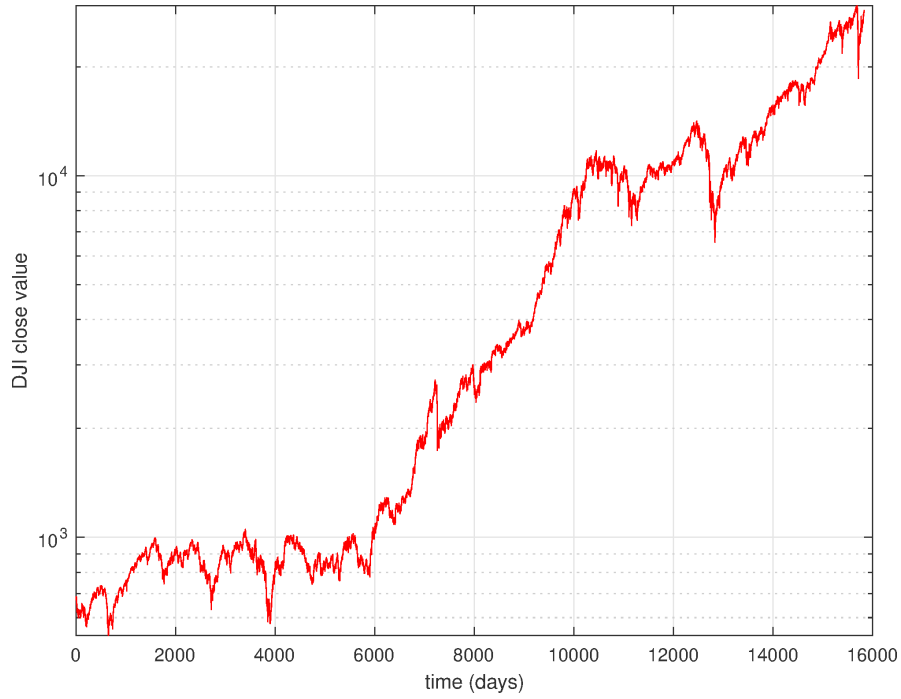

Figure 1. Daily close values of the DJIA from 28 December 1959, up to 1 September 2020.

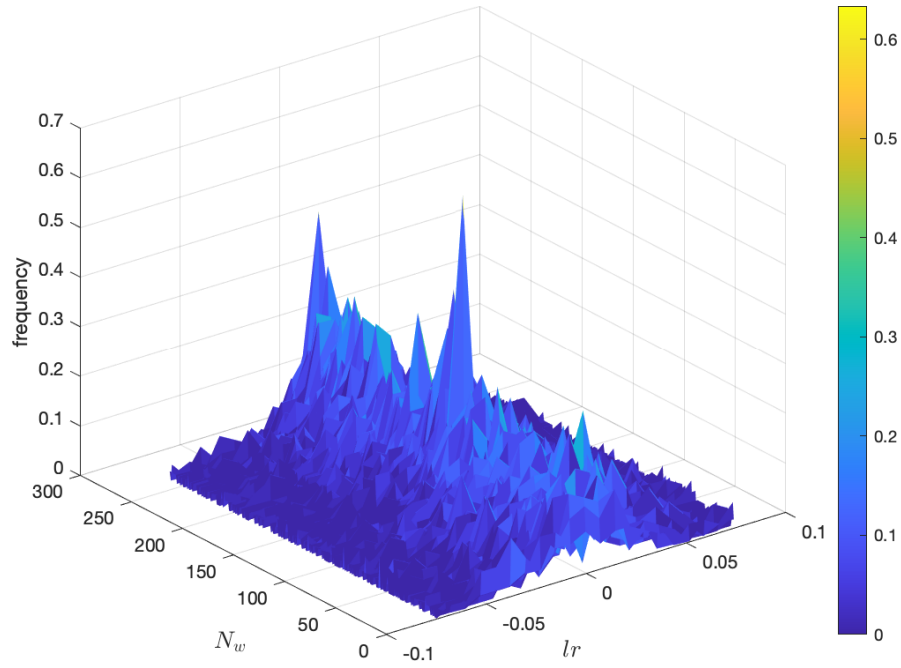

Figure 2. Histogram of the logarithm of the returns of the DJIA from 28 December 1959, up to 1 September 2020, for time windows of $t_w = 60$ days.

2.2. Distances

The DJIA dynamics is studied indirectly through the MDS by comparing the vectors $(\xi_i(1), \ldots, \xi_i(t_w))$, $i = 1, \ldots, N_w$, $t = 1, \ldots, t_w$, and analyzing the properties of the resulting plot in the perspective of entropy and fractal dimension. This approach requires the definition of an appropriate distance [62]. A function $d : \mathcal{A} \times \mathcal{A} \to \mathbb{R}$ on a set $\mathcal{A}$ is a "distance" when, for the items $\xi_i, \xi_j, \xi_k \in \mathcal{A}$, it satisfies the conditions (i) $d(\xi_i, \xi_j) \geq 0$ (non-negativity), (ii) $d(\xi_i, \xi_j) = 0$ (identity of indiscernibles) if and only if $\xi_i = \xi_j$, (iii) $d(\xi_i, \xi_j) = d(\xi_j, \xi_i)$ (symmetry), and (iv) $d(\xi_i, \xi_k) \leq d(\xi_i, \xi_j) + d(\xi_j, \xi_k)$ (triangle inequality). If the three conditions are followed, then the function is a "metric" and together

with $\mathcal{A}$ yields a "metric space". Obviously, these conditions still allow a considerable freedom, and we find in the literature a plethora of possible metrics each with its own pros and cons. In practice, users adopt one or more distances if they capture adequately the characteristics of the items under assessment. Therefore, we start by considering a test bench of 10 distinct indices, namely the Manhattan, Euclidean, Tchebychev, Lorentzian, Sørensen, Canberra, Clark, divergence, angular, and Jaccard distances (denoted as {Ma, Eu, Tc, Lo, So, Ca, Cl, Dv, Ac, Ja}), given by [63]:

$$d_{i,j}^{Ma} = \sum_{t=1}^{t_w} \left|\xi_i(t) - \xi_j(t)\right|, \tag{1a}$$

$$d_{i,j}^{Eu} = \sqrt{\sum_{t=1}^{t_w} \left(\xi_i(t) - \xi_j(t)\right)^2}, \tag{1b}$$

$$d_{i,j}^{Tc} = \max_t \left(\xi_i(t) - \xi_j(t)\right), \tag{1c}$$

$$d_{i,j}^{Lo} = \sum_{t=1}^{t_w} \log\left(1 + \left|\xi_i(t) - \xi_j(t)\right|\right), \tag{1d}$$

$$d_{i,j}^{So} = \frac{\sum_{t=1}^{t_w} \left|\xi_i(t) - \xi_j(t)\right|}{\sum_{t=1}^{t_w} \left(\left|\xi_i(t)\right| + \left|\xi_j(t)\right|\right)}, \tag{1e}$$

$$d_{i,j}^{Ca} = \sum_{t=1}^{t_w} \frac{\left|\xi_i(t) - \xi_j(t)\right|}{\left|\xi_i(t)\right| + \left|\xi_j(t)\right|}, \tag{1f}$$

$$d_{i,j}^{Cl} = \sqrt{\sum_{t=1}^{t_w} \left(\frac{\left|\xi_i(t) - \xi_j(t)\right|}{\left|\xi_i(t)\right| + \left|\xi_j(t)\right|}\right)^2}, \tag{1g}$$

$$d_{i,j}^{Dv} = \sum_{t=1}^{t_w} \frac{\left(\xi_i(t) - \xi_j(t)\right)^2}{\left(\left|\xi_i(t)\right| + \left|\xi_j(t)\right|\right)^2}, \tag{1h}$$

$$d_{i,j}^{Ac} = \arccos\left(r_{ij}\right),\ r_{ij} = \frac{\sum_{t=1}^{t_w} \xi_i(t)\xi_j(t)}{\sqrt{\sum_{t=1}^{t_w} \xi_i^2(t) \sum_{t=1}^{t_w} \xi_j^2(t)}}, \tag{1i}$$

$$d_{i,j}^{Ja} = \frac{\sum_{t=1}^{t_w} \left(\xi_i(t) - \xi_j(t)\right)^2}{\sum_{t=1}^{t_w} \xi_i^2(t) + \sum_{t=1}^{t_w} \xi_j^2(t) - \sum_{t=1}^{t_w} \xi_i(t)\xi_j(t)}, \tag{1j}$$

where ξ_i and ξ_j, $i, j = 1, \ldots, N_w$, are the ith and jth vectors of the DJIA time series, each of dimension t_w. The Manhattan, Euclidean, and Tchebychev distances are particular cases of the Minkowski distance $d_{i,j}^{Mi} = \left(\sum_{t=1}^{t_w} \left|\xi_i(t) - \xi_j(t)\right|^q\right)^{\frac{1}{q}}$, namely for $q = 1$, $q = 2$ and $q \to \infty$, respectively. The Lorentzian distance applies the natural logarithm to the absolute difference with 1 added to guarantee the non-negativity property and to eschew the log of zero. We find in the literature several distinct versions of the Sørensen distance, eventually with other names, and representing a statistic used for comparing the similarity between two samples. The Canberra and Clark distances are weighted versions of the Manhattan and Euclidean distances. These expressions replace $\left|\xi_i(t) - \xi_j(t)\right|$ by $\left|\xi(t) - \xi_j(t)\right| / \left(\left|\xi_i(t)\right| + \left|\xi_j(t)\right|\right)$ and are sensitive to small changes near zero. The angular cosine distance follows the cosine similarity r_{ij} that comes from the inner product of two vectors, $\xi_i \cdot \xi_j$. The angular

cosine distance $d_{i,j}^{Ac}$ gives the angle between the vectors ξ_i and ξ_j. The Jaccard distance is the ratio of the size of the symmetric difference to the union of two sets.

2.3. The MDS Loci

Once having defined the metric for comparing the vectors, the MDS requires the construction of a matrix $\mathbf{D} = \left[d_{i,j}\right]$ of item-to-item distances. In our case, "item" corresponds to a t_w-dim vectors. Therefore, the square matrix $\mathbf{D}$ is symmetric, with the main diagonal of zeros and dimension $N_w \times N_w$ equal to the number of items. The MDS computational algorithm tries to plot the items in a low-dimensional space so that users can easily analyze possible relationships that are difficult to unravel in a high number of dimensions. In other words, the MDS performs a dimension reduction and plots items in a $p < N_w$ dimensional space, by estimating a matrix $\hat{\mathbf{D}} = \left[\hat{d}_{i,j}\right]$, corresponding to the p-dim items $\hat{x}_i$, so that the distances, $\hat{d}_{i,j}$, mimic the original ones, $d_{i,j}$.

The classical MDS can perform the optimization procedure based on a variety of loss functions, often called "strain", that are a form of minimizing the residual sum of squares. The metric MDS generalizes the optimization procedure called "stress", S_D, such as:

$$S_D\left(\xi_1, \ldots, \xi\right) = \left[\sum_{i,j}\left(\hat{d}_{i,j} - d_{i,j}\right)^2\right]^{\frac{1}{2}}, \tag{2}$$

or:

$$S_D\left(\xi_1, \ldots, \xi\right) = \left[\frac{\sum_{i,j}\left(\hat{d}_{i,j} - d_{i,j}\right)^2}{\sum_{i,j} d_{i,j}^2}\right]^{\frac{1}{2}}, \tag{3}$$

where $d_{i,j} = \left|\xi_i - \xi_j\right|$, $i, j = 1, \ldots, N_w$.

The generalized MDS is an extension of metric formulation, so that the target space is an arbitrary smooth non-Euclidean space.

Once having obtained the MDS estimate coordinates of the objects $\hat{x}_i$, the user can decide the dimension p for visualization. Usually, the values $p = 2$ and $p = 3$ are selected since they allow a direct representation. Moreover, the quality of the MDS approximation can be assessed by means of the Sheppard and stress charts. The Sheppard diagram plots $\hat{d}_{i,j}$ vs. $d_{i,j}$. If the points follow a straight/curved line, this means a linear/non-linear relationship, but in both cases, the smaller the scatter, the better the approximation is. A second assessment tool consists of the plot of S_D vs. p. Usually, the curve is monotonic decreasing with a large diminishing at first and a slow variation afterwards.

Since the MDS locus results from relative information (i.e., the distances), the coordinates usually do not have some physical meaning, and the user can rotate, shift, or magnify the representation to have a better view. Moreover, distinct distances lead to different plots that are correct from the mathematical and computational viewpoints, but that reflect distinct characteristics of the dataset. Therefore, it is up to the user to choose one or more distances that better highlight the aspects of the dataset under study.

Often, it is recommended to pre-process the data before calculating the distances in order to reduce the sensitivity to some details such as different units or a high variation of numerical values. In the case of the DJIA, two data pre-processing schemes (also called normalizing, or data transformation), $\mathcal{P}_1$ and $\mathcal{P}_2$, are considered: (i) subtracting the arithmetic average and dividing by the standard variation, that is by calculating $\left\{\mathcal{P}_1 : x(t) \leftarrow \frac{x(t)-\mu}{\sigma}\right\}$, where $\mu = \frac{1}{T}\sum_{t=1}^{T} x(t)$ and $\sigma = \sqrt{\frac{1}{T-1}\sum_{t=1}^{T}\left(x(t)-\mu\right)^2}$, and (ii) by applying a logarithm so that $\{\mathcal{P}_2 : x(t) \leftarrow \lg\left(x\left(t\right)\right)\}$. The linear transformation $\mathcal{P}_1$ is often adopted in statistics and signal processing [64–68], while the non-linear transformation $\mathcal{P}_2$ can be adopted with signals revealing an exponential-like evolution [69–73]. Of course, other data transformations could be

envisaged, but these two are commonly adopted. Therefore, the main question concerning this issue is to understand to what extend the pre-processing influences the final results.

2.3.1. Data Pre-Processing Using $\mathcal{P}_1$

Figure 3 shows the MDS locus for $p = 3$ and $t_w = 60$ days, with pre-processing $\mathcal{P}_1$ and using the Lorentzian and Canberra distances, $d_{i,j}^{Lo}$ and $d_{i,j}^{Ca}$. The larger circle represents the first vector, and the lines connect two consecutive dots (representing the vectors from two consecutive time windows). The lines are included simply for auxiliary purposes and for highlighting the discontinuities. The MATLAB nonclassical multidimensional scaling algorithm `mdscale` and the Sammon's nonlinear mapping criterion `sammon` were used. Figure 4 illustrates the corresponding Sheppard and stress diagrams for the Canberra distance (1f). For the sake of parsimony, the other charts are not represented.

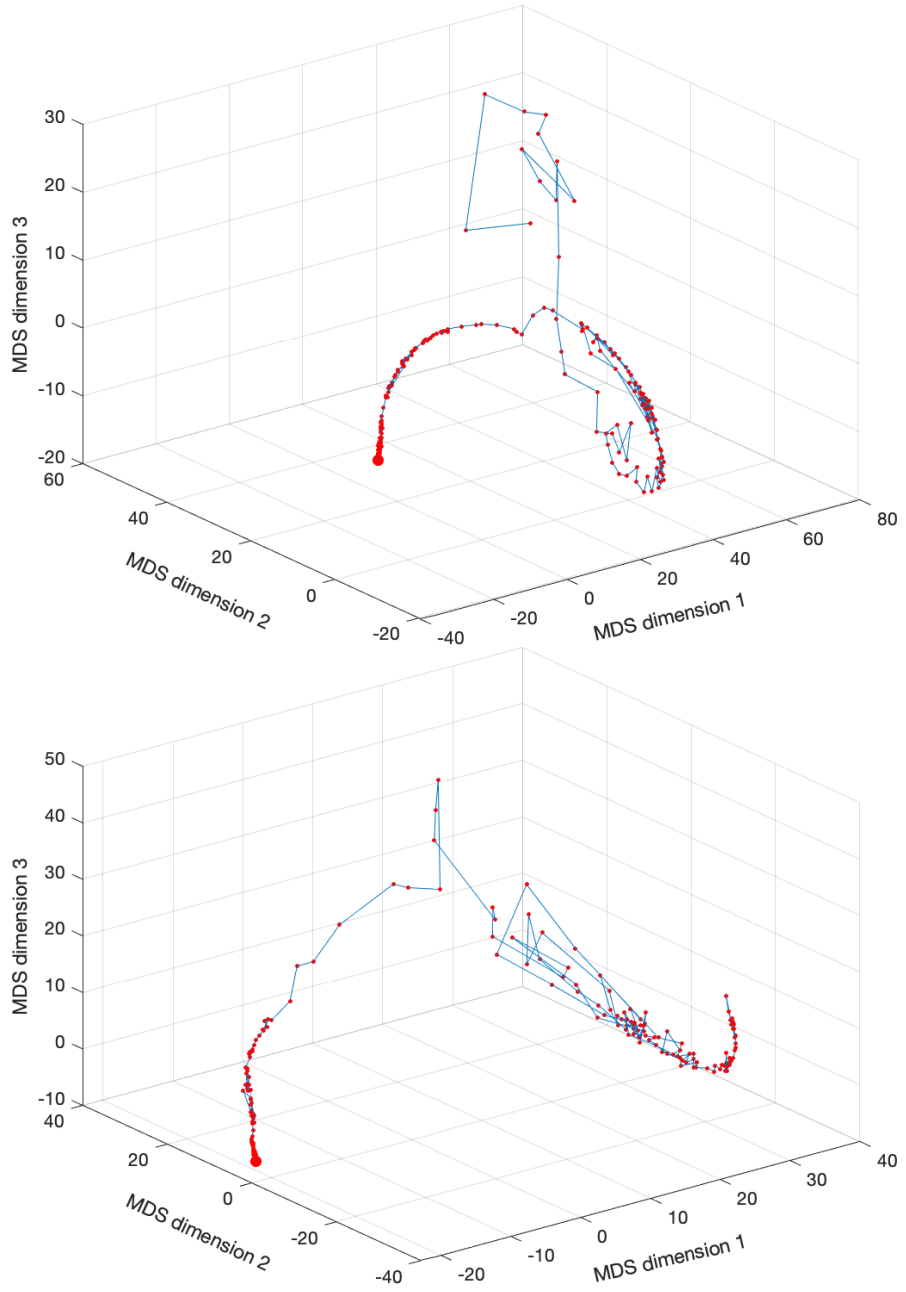

Figure 3. The multidimensional scaling (MDS) locus, $\hat{x}_i$, of the DJIA dataset for $p = 3$ and $t_w = 60$ days ($N_w = 263$), with pre-processing $\mathcal{P}_1$ and using the Lorentzian (1d) and Canberra (1f) distances.

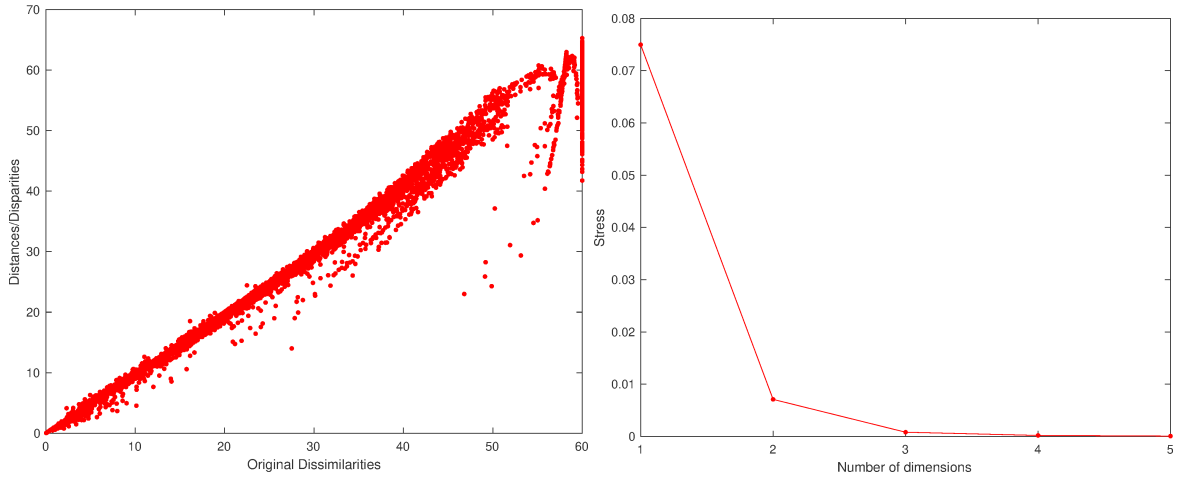

Figure 4. The Sheppard diagram, $\hat{d}_{i,j}$ vs. $d_{i,j}$, for $p = 3$, and stress plot, S_D vs. p, of the DJIA dataset with $t_w = 60$ days, with pre-processing $\mathcal{P}_1$ and using the Canberra distance (1f).

We verify that the MDS loci exhibit segments where we have an almost continuous evolution and others with strong discontinuities. The first segments portray relatively smooth dynamics, while the second ones represent dramatic variations, in the perspective of the adopted distance and visualization technique. These dynamical effects are not read in the same way as with the standard time representations. Moreover, their visualization varies according to the type of distance adopted to construct the matrix **D**. This should be expected, since it is well known that each distance highlights a specific set of properties embedded in the original time series and that the selection of one of more distances has to be performed on a case-by-case basis, before deciding those more adapted to the dataset.

Another relevant topic is the effect of the time window t_w on the results. In other words, we can ask how the dimension of the vector ξ_i, $i = 1, \ldots, N_w$, capturing the DJIA time dynamics, influences the MDS representation. For example, Figure 5 shows the MDS locus for $p = 3$, $t_w = 10$ days ($N_w = 1583$), and the Canberra distance (1e).

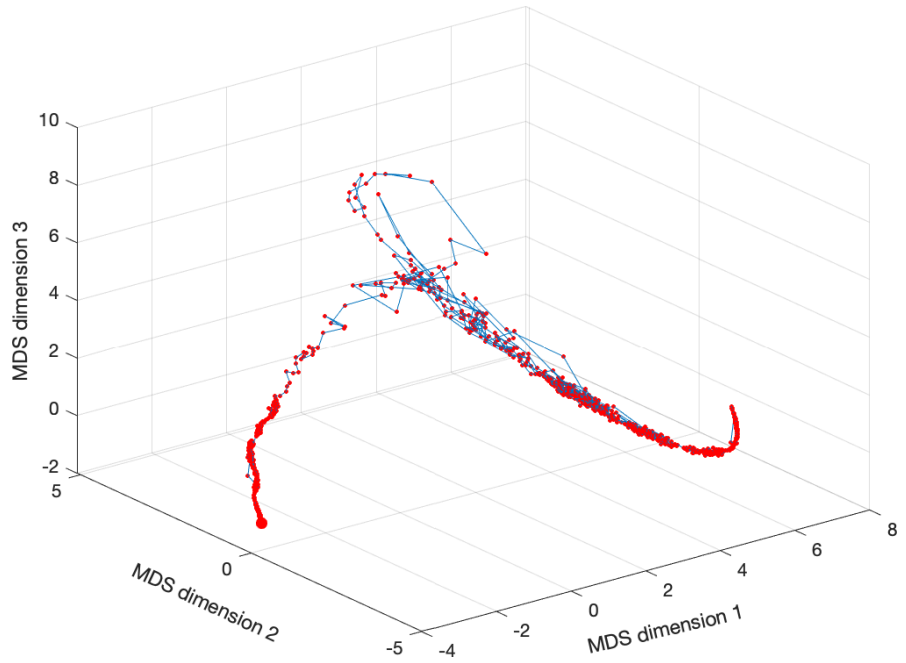

Figure 5. The MDS locus, $\hat{x}_i$, of the DJIA dataset for $p = 3$ and $t_w = 10$ days ($N_w = 1583$), with pre-processing $\mathcal{P}_1$ and using the Canberra distance (1e).

2.3.2. Data Pre-Processing Using $\mathcal{P}_2$

Figure 6 shows the MDS locus for $p = 3$ and $t_w = 60$ days, with pre-processing $\mathcal{P}_2$ and using the Lorentzian and Canberra distances, $d_{i,j}^{Lo}$ and $d_{i,j}^{Ca}$. Figure 7 depicts the Sheppard and stress diagrams for the Canberra distance (1f).

We can also check the effect of the time window t_w. Figure 8 shows the MDS locus for $p = 3$, $t_w = 10$ days ($N_w = 1583$), and the Canberra distance (1e) revealing, again, a slightly diminishing of the volatility.

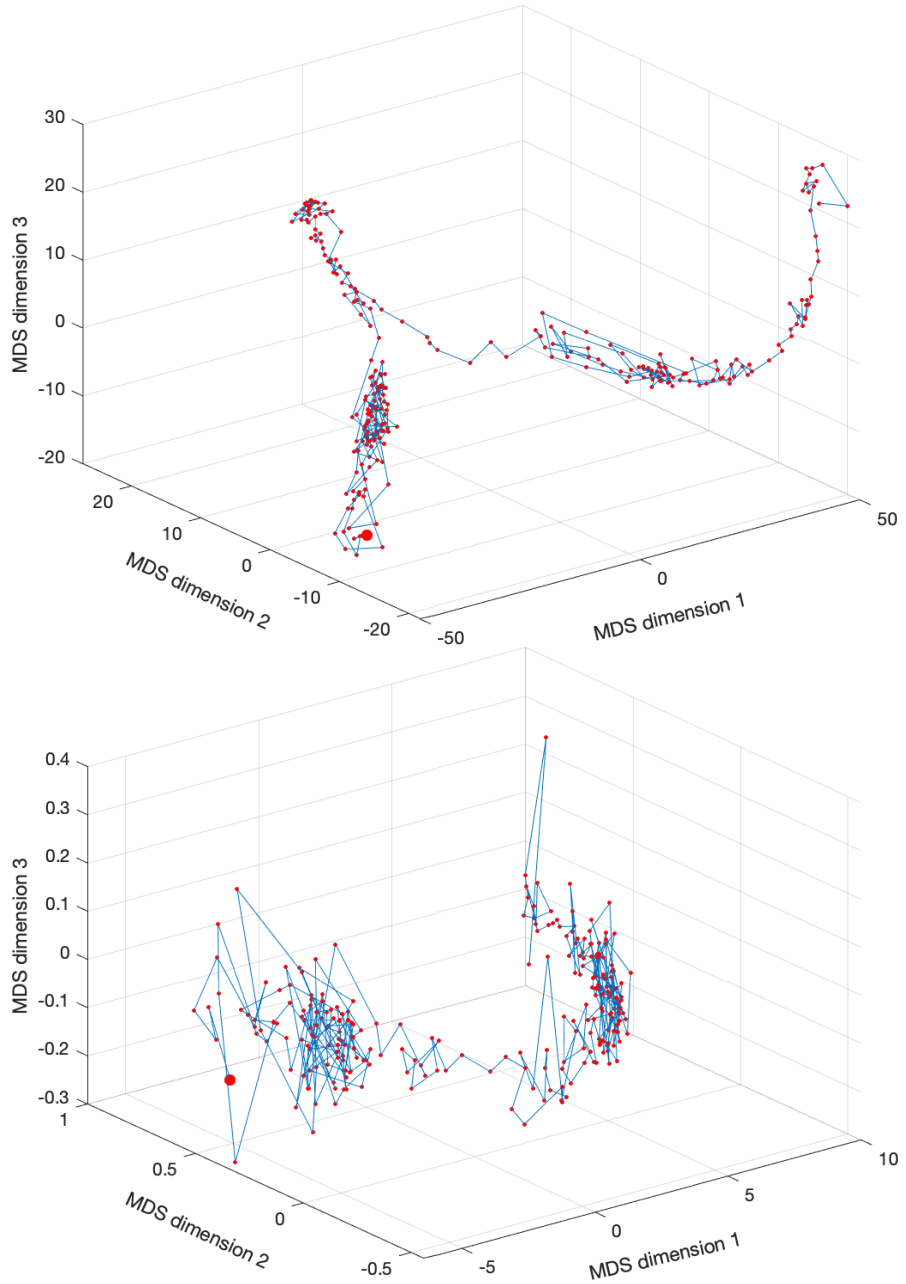

Figure 6. The MDS locus, $\hat{x}_i$, of the DJIA dataset for $p = 3$ and $t_w = 60$ days ($N_w = 263$), with pre-processing $\mathcal{P}_2$ and using the Lorentzian (1d) and Canberra (1f) distances.

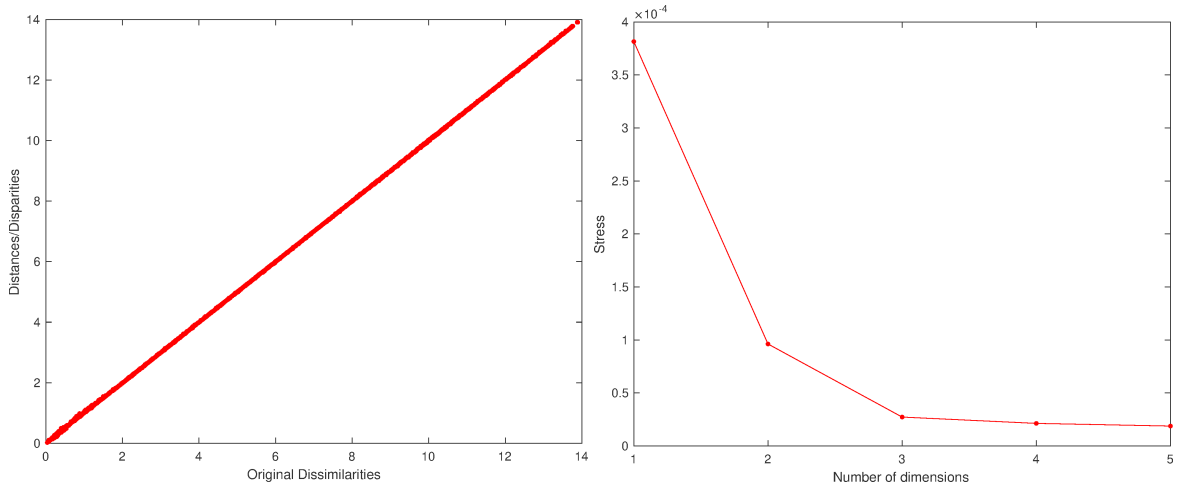

Figure 7. The Sheppard diagram, $\hat{d}_{i,j}$ vs. $d_{i,j}$, for $p = 3$, and the stress plot, S_D vs. p, of the DJIA dataset with $t_w = 60$ days, with pre-processing $\mathcal{P}_2$ and using the Canberra distance (1f).

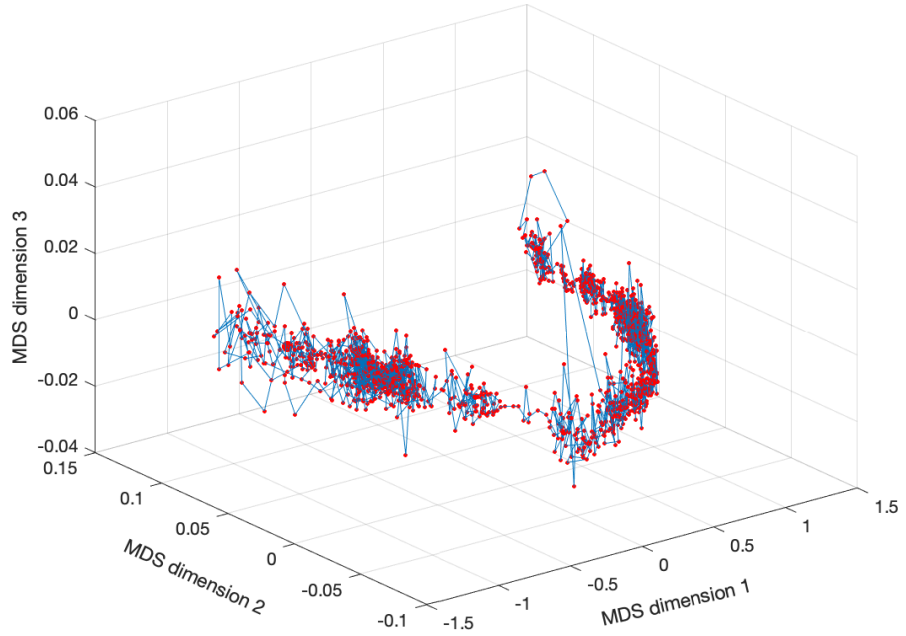

Figure 8. The MDS locus, $\hat{x}_i$, of the DJIA dataset for $p = 3$ and $t_w = 10$ days ($N_w = 1583$), with pre-processing $\mathcal{P}_2$ and using the Canberra distance (1e).

As in the previous sub-section, we observe that the MDS plots reveal some segments almost with a continuous evolution and some with discontinuities. Furthermore, as before, increasing t_w reduces the volatility in the MDS representations. These results, with regions of smooth variation, interspersed with abrupt changes, were already noticed since they reflect relativistic time effects [74,75]. Such dynamics was interpreted as a portrait of the fundamental non-smooth nature of the flow of the time variable underlying the DJIA evolution. Nonetheless, we are still far from a comprehensive understanding of the MDS loci, and we need to design additional tools to extract additional conclusions.

3. Fractal, Entropy, and Fractional Analysis

We consider the fractal dimension and entropy measures for analyzing the 3-dim portraits produced by the MDS.

The fractal dimension, f_d, characterizes the fractal pattern of a given object by quantifying the ratio of the change in detail to the change in scale. Several types of fractal dimension can be found in the literature. In our case, f_d is calculated by means of the box counting method as the exponent of

a power law $N(\epsilon) = a\epsilon^{-f_d}$, where a is a parameter that depends on the shape and size of the object, and N and ϵ stand for the number of boxes required to capture the object and the size (or scale) of the box, respectively. Therefore, f_d can be estimated as:

$$f_d = -\lim_{\epsilon \to 0} \frac{\ln(N(\epsilon))}{\ln(\epsilon)}. \tag{4}$$

The entropy of a random variable is the average level of "information" of the corresponding probability distribution. The key cornerstone of the Shannon theory consists of the information content, which for an event having probability of occurrence p_i, is given by:

$$I(p_i) = -\ln p_i. \tag{5}$$

For a 3-dim random variable (X, Y, Z) with probability distribution p_{XYZ}, the Shannon entropy, H_{XYZ}, is given by:

$$H_{XYZ} = -\sum_X \sum_Y \sum_Z p_{XYZ} \ln(p_{XYZ}), \tag{6}$$

where $-\ln(p_{XYZ})$ is the information for the event with probability p_{XYZ}.

The concept of entropy can be generalized in the scope of fractional calculus [76–86]. This approach gives more freedom to adapt the entropy measure to the phenomenon under study by adjusting the fractional order. The information and entropy of order $\alpha \in \mathbb{R}$ are given by [77,87]:

$$I_\alpha(p_i) = D^\alpha I(p_i) = -\frac{p_i^{-\alpha}}{\Gamma(\alpha+1)} [\ln p_i + \psi(1) - \psi(1-\alpha)] \tag{7}$$

$$H^\alpha_{XYZ} = \sum_i \left\{ -\frac{p_i^{-\alpha}}{\Gamma(\alpha+1)} [\ln p_i + \psi(1) - \psi(1-\alpha)] \right\} p_i \tag{8}$$

where $\Gamma(\cdot)$ and $\psi(\cdot)$ represent the gamma and digamma functions.

The parameter α gives an extra degree of freedom to adapt the sensitivity of the entropy calculation of each specific data series.

In an algorithmic perspective, these measures require the adoption of some grid (or box) for capturing and counting the objects, the main difference being that the fractal dimension just considers a Boolean perspective of "1" and "0", that is the box is either full or empty, while the entropy considers the number of counts in each box.

In the follow-up, a 3-dim grid defined between the minimum and maximum values obtained for each axis of the MDS locus is considered. For the fractal dimension, we obtain f_d by the slope of $N(\epsilon)$ versus ϵ for 10 decreasing values of the box sizes. In the case of the entropy, we calculate H_{XYZ} when adopting 20 bins for each MDS axis. The auxiliary lines connecting the object (i.e., the points) are not considered for the calculations.

Figures 9 and 10 show the variation of f_d and H_{XYZ} with t_w, with pre-processing $\mathcal{P}_1$ and $\mathcal{P}_2$, respectively, when using the distances (1a)–(1j). For $t_w \in \{5, \ldots, 240\}$, we have correspondingly MDS with N_w ($t_w \in \{3166, \ldots, 65\}$) points.

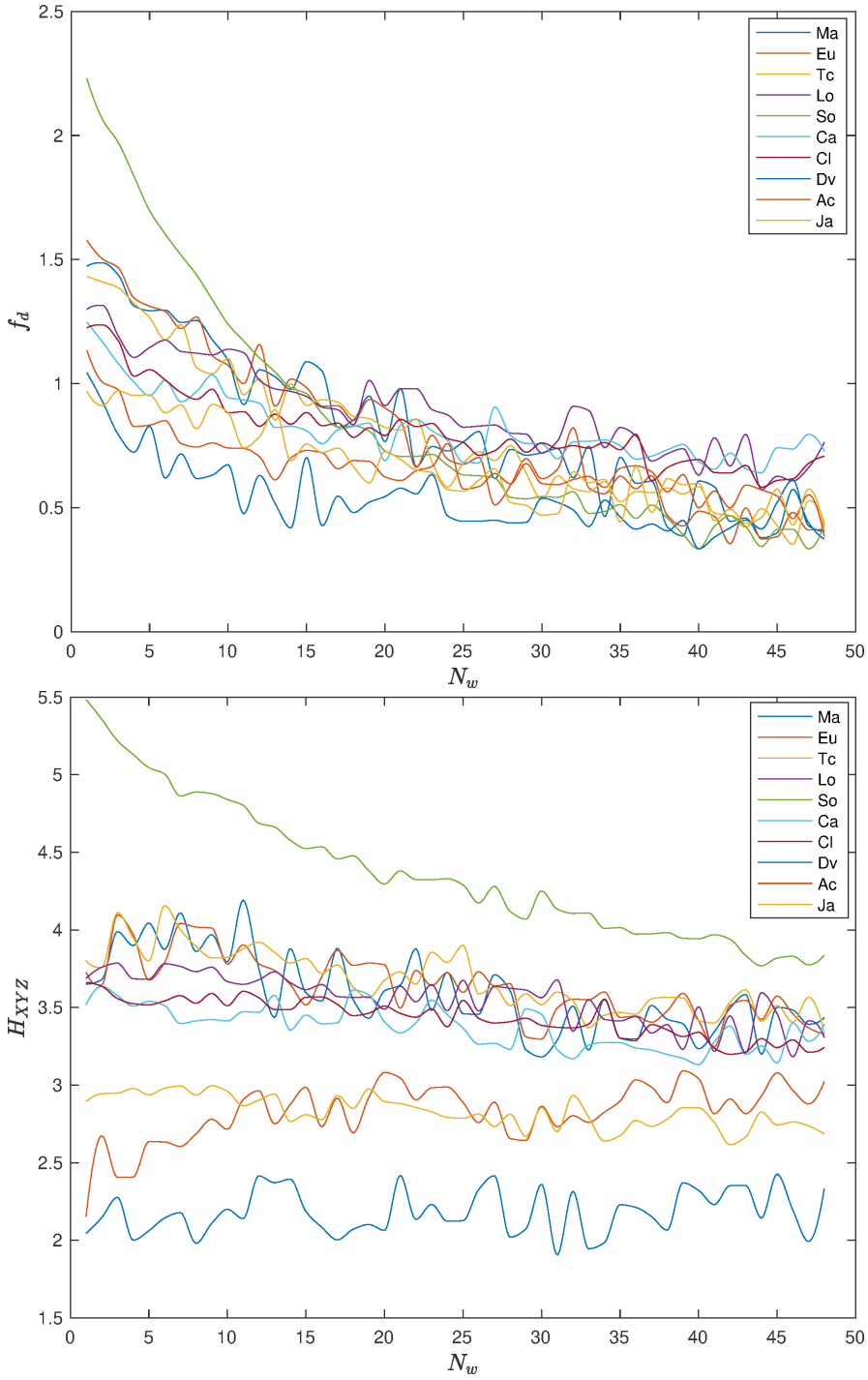

Figure 9. Plot of fractal dimension, f_d, and Shannon entropy, H_{XYZ}, versus N_w ($t_w \in \{5, \ldots, 240\}$), with pre-processing $\mathcal{P}_1$ and using the distances (1a)–(1j).

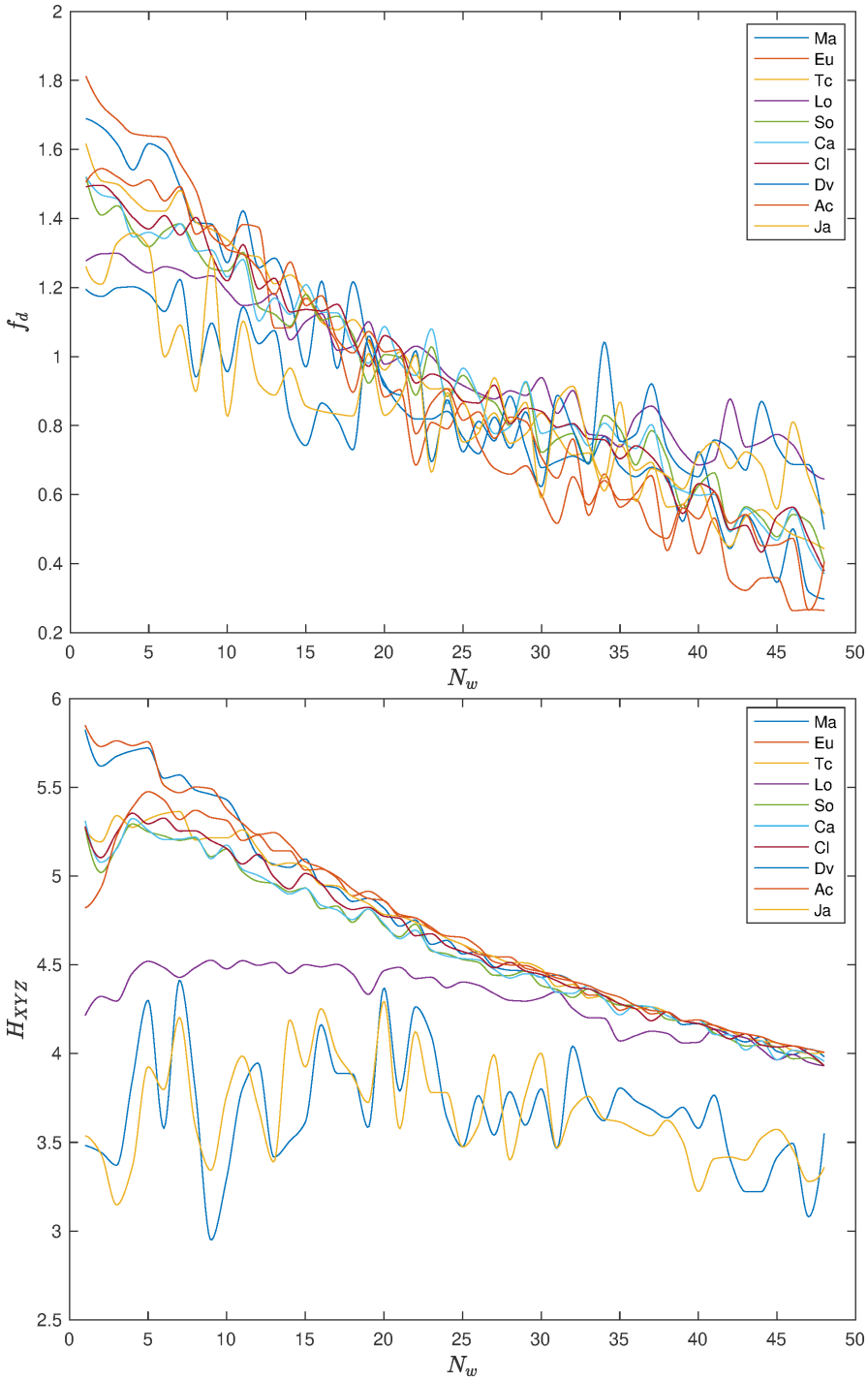

Figure 10. Plot of fractal dimension, f_d, and Shannon entropy, H_{XYZ}, versus N_w ($t_w \in \{5, \ldots, 240\}$), with pre-processing $\mathcal{P}_2$ and using the distances (1a)–(1j). The Manhattan, Euclidean, Tchebychev, Lorentzian, Sørensen, Canberra, Clark, divergence, angular, and Jaccard distances (denoted as {Ma, Eu, Tc, Lo, So, Ca, Cl, Dv, Ac, Ja}).

We note some "noise", but that should be expected due to the numerical nature of the experiments. In general, the two indices decrease with t_w, revealing, again, the "low pass filtering" effect of the dimension of the time window. We note a considerable difference of the values of f_d and H_{XYZ} for small values of t_w, but a stabilization and some convergence to closer values when t_w increases.

In the case of the fractional entropy, H^{α}_{XYZ}, we can tune the value of α to achieve a maximum sensitivity. In other words, we can select the value $\alpha_{max(H)}$ to obtain max $\left(H^{\alpha}_{XYZ}\right)$. Figures 11 and 12

depict max $\left(H^{\alpha}_{XYZ}\right)$ vs. $\alpha_{max(H)}$ with $t_w \in \{5, 10, \ldots, 240\}$, with pre-processing $\mathcal{P}_1$ and $\mathcal{P}_2$, respectively, and using the distances (1a)–(1j).

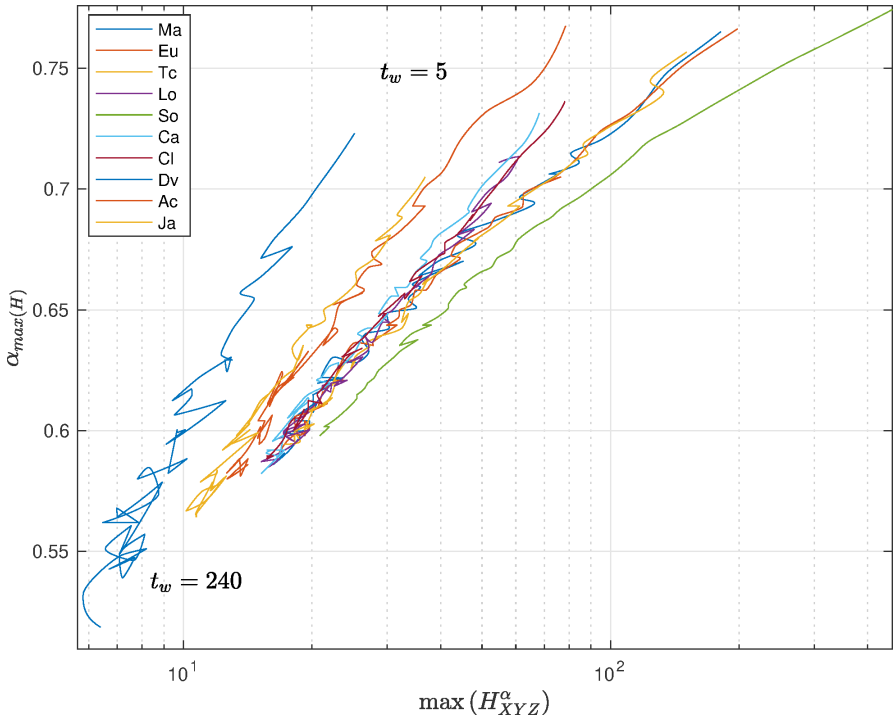

Figure 11. Plot of $\alpha_{max(H)}$ versus max $\left(H^{\alpha}_{XYZ}\right)$, with $t_w \in \{5, 10, \ldots, 240\}$, with pre-processing $\mathcal{P}_1$ and using the distances (1a)–(1j).

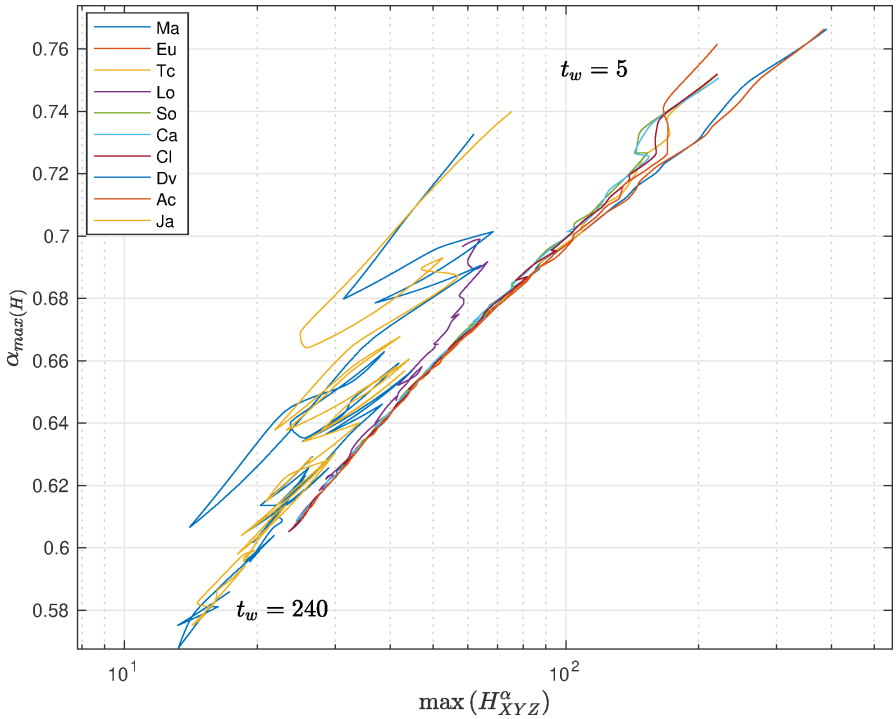

Figure 12. Plot of $\alpha_{max(H)}$ versus max $\left(H^{\alpha}_{XYZ}\right)$, with $t_w \in \{5, 10, \ldots, 240\}$, with pre-processing $\mathcal{P}_2$ and using the distances (1a)–(1j).

We verify a strong correlation between the entropy and the value of the fractional order. Furthermore, we note that $0.55 \leq \alpha_{max(H)} \leq 0.75$ and $0.57 \leq \alpha_{max(H)} \leq 0.77$ for $\mathcal{P}_1$ and $\mathcal{P}_2$, respectively, far from integer values and clearly representative of fractional dynamics. For small time windows, each distance has a distinct behavior, but when the time window increases, all distances converge to almost similar points of $\alpha_{max(H)}$, both for $\mathcal{P}_1$ and $\mathcal{P}_2$. Obviously, with larger time windows, we have a smaller number of points in the MDS locus, and that influences the result. The convergence towards a common behavior for all distances is observed after the first values of t_w. This means that we are unraveling the fractional dynamics, that is a characteristic of long-range memory effects embedded in the time series.

For the pre-processing $\mathcal{P}_1$, the divergence distance produces a slightly separated plot to the left, while for $\mathcal{P}_2$, we see that position is occupied the divergence and Jaccard distances, but with a fuzzier behavior. As before, we note that the type of pre-processing does not yield any significant modification of the global conclusions.

4. Conclusions

Commonly, time is viewed as a continuous and linear flow so that any perturbation, such as noise and volatility, is automatically assigned to the variable under analysis. In other words, since we are entities immersed in the time flow, apparently, we are incapable of distinguishing between perturbations in the time and the measured variable. This paper explored an alternative strategy of reading the relationship between the variables. For that purpose, the DJIA, from 28 December 1959, up to 1 September 2020, was adopted as the vehicle for the numerical experiments. This dataset corresponds to a human-made phenomenon, and therefore, any conjecture about the nature of time is independent of the presently accepted conceptions about its flux. In the proposed approach, the time series was organized into vectors corresponding to specified time windows. Those vectors were then compared by means of a panoply of distances and the resulting information plotted in a three-dimensional space by means of MDS. Indeed, the MDS representation corresponds to a "customized projection" of high-dimensional data into a low-dimensional space. Loosely speaking, we can say "customized projection" since we do not pose any a priori requirements, the algorithm merely being based on the idea of minimizing the difference between the original measurements and the replicated (approximated) value. Therefore, the MDS does not automatically guarantee the success of such a "projection", but the quality results were assessed by the stress and Shepard diagrams. In the case of the DJIA and the adopted distances, the good quality of the MDS technique was confirmed.

The MDS loci have distinct shapes, according to the type of distance adopted to compare vectors. Therefore, additional tools were necessary to highlight the main characteristics of these representations where time is no longer the explicit variable. For that purpose, several mathematical tools were considered, namely the Shannon entropy and fractal dimension. In all cases, we observed some variability with the time window, which occurs naturally due to the numerical treatment of this type of data. The Shannon entropy and fractal dimension exhibited the same type of behavior, with a progressive variation with the time window and a stabilization toward a common value for large t_w. While these results can be read merely as the effect of a low pass filtering provided by the large time window, we can also foresee that another property inherent to the DJIA is their origin.

The fractional entropy was brought up to further analyze the MDS locus. This tool allows a better sensitivity to the dataset than the Shannon entropy, since users can tune the calculations by means of the fractional order. In the case of the DJIA, the tuning of α for achieving the maximum entropy revealed not only that such values are independent of the distance, but also that we clearly have orders far from integer values, characteristic of fractional dynamics with non-local effects.

Some concepts are debatable and do not follow the standard orthodoxy, but the set of experiments with an artificial time series allows thinking outside the box and provides a strategy for exploring the texture of time in the perspective of entropy and fractional calculus.

Funding: This research received no external funding.

Conflicts of Interest: The author declares no conflict of interest.

References

1. Trippi, R. *Chaos & Nonlinear Dynamics in the Financial Markets*; Irwin Professional Publishing Company: Burr Ridge, IL, USA, 1995.
2. Vialar, T. *Complex and Chaotic Nonlinear Dynamics: Advances in Economics and Finance, Mathematics and Statistics*; Springer: Berlin/Heidelberg, Germany, 2009.
3. Bischi, G.I.; Chiarella, C.; Gardini, L. (Eds.) *Nonlinear Dynamics in Economics, Finance and the Social Sciences*; Springer: Berlin/Heidelberg, Germany, 2010.
4. Meyers, R.A. (Ed.) *Complex Systems in Finance and Econometrics*; Springer: New York, NY, USA, 2010.
5. Machado, J.A.T. Calculation of Fractional Derivatives of Noisy Data with Genetic Algorithms. *Nonlinear Dyn.* **2009**, *57*, 253–260. [CrossRef]
6. Duarte, F.B.; Machado, J.A.T.; Duarte, G.M. Dynamics of the Dow Jones and the NASDAQ Stock Indexes. *Nonlinear Dyn.* **2010**, *61*, 691–705. [CrossRef]
7. Machado, J.T.; Duarte, F.B.; Duarte, G.M. Analysis of stock market indices through multidimensional scaling. *Commun. Nonlinear Sci. Numer. Simul.* **2011**, *16*, 4610–4618. [CrossRef]
8. Machado, J.A.T.; Duarte, G.M.; Duarte, F.B. Analysis of Financial Data Series Using Fractional Fourier Transform and Multidimensional Scaling. *Nonlinear Dyn.* **2011**, *65*, 235–245. [CrossRef]
9. Machado, J.A.T.; Duarte, G.M.; Duarte, F.B. Identifying Economic Periods and Crisis with the Multidimensional Scaling. *Nonlinear Dyn.* **2011**, *63*, 611–622. [CrossRef]
10. Machado, J.T.; Duarte, F.B.; Duarte, G.M. Analysis of Financial Indices by Means of The Windowed Fourier Transform. *Signal Image Video Process.* **2012**, *6*, 487–494. [CrossRef]
11. Machado, J.T.; Duarte, G.M.; Duarte, F.B. Analysis of stock market indices with multidimensional scaling and wavelets. *Math. Probl. Eng.* **2012**, *2012*, 14.
12. Machado, J.A.T.; Duarte, G.M.; Duarte, F.B. Fractional dynamics in financial indexes. *Int. J. Bifurc. Chaos* **2012**, *22*, 1250249. [CrossRef]
13. Machado, J.T.; Duarte, F.B.; Duarte, G.M. Power Law Analysis of Financial Index Dynamics. *Discret. Dyn. Nat. Soc.* **2012**, *2012*, 12.
14. Da Silva, S.; Matsushita, R.; Gleria, I.; Figueiredo, A.; Rathie, P. International finance, Lévy distributions, and the econophysics of exchange rates. *Commun. Nonlinear Sci. Numer. Simul.* **2005**, *10*, 355–466. [CrossRef]
15. Chen, W.C. Nonlinear dynamics and chaos in a fractional-order financial system. *Chaos Solitons Fractals* **2008**, *36*, 1305–1314. [CrossRef]
16. Piqueira, J.R.C.; Mortoza, L.P.D. Complexity analysis research of financial and economic system under the condition of three parameters' change circumstances. *Commun. Nonlinear Sci. Numer. Simul.* **2012**, *17*, 1690–1695. [CrossRef]
17. Ma, J.; Bangura, H.I. Complexity analysis research of financial and economic system under the condition of three parameters' change circumstances. *Nonlinear Dyn.* **2012**, *70*, 2313–2326. [CrossRef]
18. Ngounda, E.; Patidar, K.C.; Pindza, E. Contour integral method for European options with jumps. *Commun. Nonlinear Sci. Numer. Simul.* **2013**, *18*, 478–492. [CrossRef]
19. Horwich, P. *Asymmetries in Time: Problems in the Philosophy of Science*; The MIT Press: Cambridge, MA, USA, 1987.
20. Reichenbach, H. *The Direction of Time*; University of California Press: New York, NY, USA, 1991.
21. Dainton, B. *Time and Space*, 2nd ed.; Acumen Publishing, Limited: Chesham, UK, 2001.
22. Callender, C. (Ed.) *The Oxford Handbook of Philosophy of Time*; Oxford University Press: New York, NY, USA, 2011.
23. Torgerson, W. *Theory and Methods of Scaling*; Wiley: New York, NY, USA, 1958.
24. Shepard, R.N. The analysis of proximities: Multidimensional scaling with an unknown distance function. *Psychometrika* **1962**, *27*, 219–246. [CrossRef]

25. Kruskal, J. Multidimensional scaling by optimizing goodness of fit to a nonmetric hypothesis. *Psychometrika* **1964**, *29*, 1–27. [CrossRef]
26. Sammon, J. A nonlinear mapping for data structure analysis. *IEEE Trans. Comput.* **1969**, *18*, 401–409. [CrossRef]
27. Kruskal, J.B.; Wish, M. *Multidimensional Scaling*; Sage Publications: Newbury Park, CA, USA, 1978.
28. Borg, I.; Groenen, P.J. *Modern Multidimensional Scaling-Theory and Applications*; Springer: New York, NY, USA, 2005.
29. Saeed, N.; Nam, H.; Imtiaz, M.; Saqib, D.B.M. A Survey on Multidimensional Scaling. *ACM Comput. Surv. CSUR* **2018**, *51*, 47. [CrossRef]
30. Mandelbrot, B.B.; Ness, J.W.V. The fractional Brownian motions, fractional noises and applications. *SIAM Rev.* **1968**, *10*, 422–437. [CrossRef]
31. Mandelbrot, B.B. *The Fractal Geometry of Nature*; W. H. Freeman: New York, NY, USA, 1983.
32. Berry, M.V. Diffractals. *J. Phys. A Math. Gen.* **1979**, *12*, 781–797. [CrossRef]
33. Lapidus, M.L.; Fleckinger-Pellé, J. Tambour fractal: Vers une résolution de la conjecture de Weyl-Berry pour les valeurs propres du Laplacien. *C. R. L'Académie Sci. Paris Sér. I Math.* **1988**, *306*, 171–175.
34. Schroeder, M. *Fractals, Chaos, Power Laws: Minutes from an Infinite Paradise*; W. H. Freeman: New York, NY, USA, 1991.
35. Shannon, C.E. A mathematical theory of communication. *Bell Syst. Tech. J.* **1948**, *27*, 379–423, 623–656. [CrossRef]
36. Khinchin, A.I. *Mathematical Foundations of Information Theory*; Dover: New York, NY, USA, 1957.
37. Jaynes, E.T. Information Theory and Statistical Mechanics. *Phys. Rev.* **1957**, *106*, 620–630. [CrossRef]
38. Rényi, A. On measures of information and entropy. In *Proceedings of the fourth Berkeley Symposium on Mathematics, Statistics and Probability, Volume 1: Contributions to the Theory of Statistics, Berkeley, CA, USA, 20 June–30 July 1960*; University of California Press: Berkeley, CA, USA, 1961; pp. 547–561. Available online: https://projecteuclid.org/euclid.bsmsp/1200512181 (accessed on 4 September 2020).
39. Brillouin, L. *Science and Information Theory*; Academic Press: London, UK, 1962.
40. Lin, J. Divergence measures based on the Shannon entropy. *IEEE Trans. Inf. Theory* **1991**, *37*, 145–151. [CrossRef]
41. Beck, C. Generalised information and entropy measures in physics. *Contemp. Phys.* **2009**, *50*, 495–510. [CrossRef]
42. Gray, R.M. *Entropy and Information Theory*; Springer: New York, NY, USA, 2011.
43. Oldham, K.; Spanier, J. *The Fractional Calculus: Theory and Application of Differentiation and Integration to Arbitrary Order*; Academic Press: New York, NY, USA, 1974.
44. Samko, S.; Kilbas, A.; Marichev, O. *Fractional Integrals and Derivatives: Theory and Applications*; Gordon and Breach Science Publishers: Amsterdam, The Netherlands, 1993.
45. Miller, K.; Ross, B. *An Introduction to the Fractional Calculus and Fractional Differential Equations*; John Wiley and Sons: New York, NY, USA, 1993.
46. Kilbas, A.; Srivastava, H.; Trujillo, J. Volume 204, North-Holland Mathematics Studies. In *Theory and Applications of Fractional Differential Equations*; Elsevier: Amsterdam, The Netherlands, 2006.
47. Kochubei, A.; Luchko, Y. (Eds.) Volume 1, De Gruyter Reference. In *Handbook of Fractional Calculus with Applications: Basic Theory*; De Gruyter: Berlin, Germany, 2019.
48. Kochubei, A.; Luchko, Y. (Eds.) Volume 2, De Gruyter Reference. In *Handbook of Fractional Calculus with Applications: Fractional Differential Equations*; De Gruyter: Berlin, Germany, 2019.
49. Westerlund, S.; Ekstam, L. Capacitor theory. *IEEE Trans. Dielectr. Electr. Insul.* **1994**, *1*, 826–839. [CrossRef]
50. Grigolini, P.; Aquino, G.; Bologna, M.; Luković, M.; West, B.J. A theory of $1/f$ noise in human cognition. *Phys. A Stat. Mech. Its Appl.* **2009**, *388*, 4192–4204. [CrossRef]
51. West, B.J.; Grigolini, P. *Complex Webs: Anticipating the Improbable*; Cambridge University Press: New York, NY, USA, 2010.
52. Tarasov, V. *Fractional Dynamics: Applications of Fractional Calculus to Dynamics of Particles, Fields and Media*; Springer: New York, NY, USA, 2010.
53. Mainardi, F. *Fractional Calculus and Waves in Linear Viscoelasticity: An Introduction to Mathematical Models*; Imperial College Press: London, UK, 2010.

54. Ortigueira, M.D. *Fractional Calculus for Scientists and Engineers*; Lecture Notes in Electrical Engineering; Springer: Dordrecht, The Netherlands, 2011.
55. West, B.J. *Fractional Calculus View of Complexity: Tomorrow's Science*; CRC Press: Boca Raton, FL, USA, 2015.
56. Tarasov, V.E. (Ed.) Volume 4, De Gruyter Reference. In *Handbook of Fractional Calculus with Applications: Applications in Physics, Part A*; De Gruyter: Berlin, Germany, 2019.
57. Tarasov, V.E. (Ed.) Volume 5, De Gruyter Reference. In *Handbook of Fractional Calculus with Applications: Applications in Physics, Part B*; De Gruyter: Berlin, Germany, 2019.
58. Machado, J.A.T.; Mata, M.E. A multidimensional scaling perspective of Rostow's forecasts with the track-record (1960s–2011) of pioneers and latecomers. In *Dynamical Systems: Theory, Proceedings of the 12th International Conference on Dynamical Systems—Theory and Applications*; Awrejcewicz, J., Kazmierczak, M., Olejnik, P., Mrozowski, J., Eds.; Łódź University of Technology: Łódź, Poland, 2013; pp. 361–378.
59. Machado, J.A.T.; Mata, M.E. Analysis of World Economic Variables Using Multidimensional Scaling. *PLoS ONE* **2013**, *10*, e0121277. [CrossRef]
60. Tenreiro Machado, J.A.; Lopes, A.M.; Galhano, A.M. Multidimensional scaling visualization using parametric similarity indices. *Entropy* **2015**, *17*, 1775–1794. [CrossRef]
61. Mata, M.; Machado, J. Entropy Analysis of Monetary Unions. *Entropy* **2017**, *19*, 245. [CrossRef]
62. Deza, M.M.; Deza, E. *Encyclopedia of Distances*; Springer: Berlin/Heidelberg, Germany, 2009.
63. Cha, S.H. Measures between Probability Density Functions. *Int. J. Math. Model. Methods Appl. Sci.* **2007**, *1*, 300–307.
64. Papoulis, A. *Signal Analysis*; McGraw-Hill: New York, NY, USA, 1977.
65. Oppenheim, A.V.; Schafer, R.W. *Digital Signal Processing*; Prentice Hall: Upper Saddle River, NJ, USA, 1989.
66. Parzen, E. *Modern Probability Theory and Its Applications*; Wiley-Interscience: New York, NY, USA, 1992.
67. Pollock, D.S.; Green, R.C.; Nguyen, T. (Eds.) *Handbook of Time Series Analysis, Signal Processing, and Dynamics (Signal Processing and Its Applications)*; Academic Press: London, UK, 1999.
68. Small, M. *Applied Nonlinear Time Series Analysis: Applications in Physics, Physiology and Finance*; World Scientific Publishing: Singapore, 2005.
69. Keene, O.N. The log transformation is special. *Stat. Med.* **1995**, *14*, 811–819. [CrossRef] [PubMed]
70. Leydesdorff, L.; Bensman, S. Classification and powerlaws: The logarithmic transformation. *J. Am. Soc. Inf. Sci. Technol.* **2006**, *57*, 1470–1486. [CrossRef]
71. Stango, V.; Zinman, J. Exponential Growth Bias and Household Finance. *J. Financ.* **2009**, *64*, 2807–2849. [CrossRef]
72. Feng, C.; Wang, H.; Lu, N.; Chen, T.; He, H.; Lu, Y.; Tu, X.M. Log-transformation and its implications for data analysis. *Shanghai Arch. Psychiatry* **2014**, *26*, 105–109. [CrossRef] [PubMed]
73. Lopes, A.; Machado, J.T.; Galhano, A. Empirical Laws and Foreseeing the Future of Technological Progress. *Entropy* **2016**, *18*, 217. [CrossRef]
74. Machado, J.A.T. Complex Dynamics of Financial Indices. *Nonlinear Dyn.* **2013**, *74*, 287–296. [CrossRef]
75. Machado, J.A.T. Relativistic Time Effects in Financial Dynamics. *Nonlinear Dyn.* **2014**, *75*, 735–744. [CrossRef]
76. Ubriaco, M.R. Entropies based on fractional calculus. *Phys. Lett. A* **2009**, *373*, 2516–2519. [CrossRef]
77. Machado, J.A.T. Fractional Order Generalized Information. *Entropy* **2014**, *16*, 2350–2361. [CrossRef]
78. Karci, A. Fractional order entropy: New perspectives. *Optik* **2016**, *127*, 9172–9177. [CrossRef]
79. Bagci, G.B. The third law of thermodynamics and the fractional entropies. *Phys. Lett. A* **2016**, *380*, 2615–2618. [CrossRef]
80. Xu, J.; Dang, C. A novel fractional moments-based maximum entropy method for high-dimensional reliability analysis. *Appl. Math. Model.* **2019**, *75*, 749–768. [CrossRef]
81. Xu, M.; Shang, P.; Qi, Y.; Zhang, S. Multiscale fractional order generalized information of financial time series based on similarity distribution entropy. *Chaos Interdiscip. J. Nonlinear Sci.* **2019**, *29*, 053108. [CrossRef] [PubMed]
82. Machado, J.A.T.; Lopes, A.M. Fractional Rényi entropy. *Eur. Phys. J. Plus* **2019**, *134*. [CrossRef]
83. Ferreira, R.A.C.; Machado, J.T. An Entropy Formulation Based on the Generalized Liouville Fractional Derivative. *Entropy* **2019**, *21*, 638. [CrossRef]
84. Matouk, A. Complex dynamics in susceptible-infected models for COVID-19 with multi-drug resistance. *Chaos Solitons Fractals* **2020**, *140*, 110257. [CrossRef]

85. Matouk, A.; Khan, I. Complex dynamics and control of a novel physical model using nonlocal fractional differential operator with singular kernel. *J. Adv. Res.* **2020**, *24*, 463–474. [CrossRef]
86. Matouk, A.E. (Ed.) *Advanced Applications of Fractional Differential Operators to Science and Technology*; IGI Global: Hershey, PA, USA, 2020. [CrossRef]
87. Valério, D.; Trujillo, J.J.; Rivero, M.; Machado, J.T.; Baleanu, D. Fractional Calculus: A Survey of Useful Formulas. *Eur. Phys. J. Spec. Top.* **2013**, *222*, 1827–1846. [CrossRef]